

RSC Advances



This is an *Accepted Manuscript*, which has been through the Royal Society of Chemistry peer review process and has been accepted for publication.

Accepted Manuscripts are published online shortly after acceptance, before technical editing, formatting and proof reading. Using this free service, authors can make their results available to the community, in citable form, before we publish the edited article. This *Accepted Manuscript* will be replaced by the edited, formatted and paginated article as soon as this is available.

You can find more information about *Accepted Manuscripts* in the [Information for Authors](#).

Please note that technical editing may introduce minor changes to the text and/or graphics, which may alter content. The journal's standard [Terms & Conditions](#) and the [Ethical guidelines](#) still apply. In no event shall the Royal Society of Chemistry be held responsible for any errors or omissions in this *Accepted Manuscript* or any consequences arising from the use of any information it contains.

Hydrothermal synthesis of Ni₃S₂/graphene electrode and its application in supercapacitor

Zhen Zhang, Xuejun Liu, Xiang Qi*, Zongyu Huang, Long Ren, Jianxin Zhong

Hunan Key Laboratory of Micro-Nano Energy Materials and Devices, Xiangtan University, Hunan 411105, P.R. China, and Laboratory for Quantum Engineering and Micro-Nano Energy Technology and Faculty of Materials and Optoelectronic Physics, Xiangtan University, Hunan 411105, P. R. China

* Corresponding author: Faculty of Materials and Optoelectronic Physics, Xiangtan University,

Hunan 411105, P. R. China

E-mail address: xqi@xtu.edu.cn (X. Qi)

Abstract

In this work, we demonstrate a simple hydrothermal synthesis of nickel sulfide/graphene nanosheets ($\text{Ni}_3\text{S}_2/\text{GNS}$), and use the nanocomposite as an electrode for supercapacitor. X-ray diffraction, scanning electron microscopy and Raman spectroscopy are used to investigate the morphologies and microstructures of the resulting electrode materials. Detail electrochemical characterization shows that the $\text{Ni}_3\text{S}_2/\text{GNS}$ electrode exhibits high specific capacitance of about 1420 Fg^{-1} at the current density of 2 Ag^{-1} . At a current density of 6 Ag^{-1} , the specific capacitance of $\text{Ni}_3\text{S}_2/\text{GNS}$ electrode fairly keeps constant with the initial value after 2000 cycles, obviously illustrating a relatively high cycling stability. The outstanding electrochemical properties of the $\text{Ni}_3\text{S}_2/\text{GNS}$ nanocomposite suggest that it has great practical potentially applications for high-performance supercapacitors.

Keywords: Ni_3S_2 ; Graphene; Electrochemical; Supercapacitor

1. Introduction

As a rising star, graphene has attracted the most intensive attention recently, due to its high specific surface area of $2600 \text{ m}^2\text{g}^{-1}$, high electrical conductivity, chemical stability and excellent mechanical properties.^{1, 2} These outstanding properties guarantee its potentially significant utility in many fields, such as field-effect transistors, rechargeable lithium-ion batteries, fuel cells, solar cells, supercapacitor and electrochemical sensors.³⁻¹⁷ Among them, supercapacitor, also known as electrochemical capacitor, is anticipated to have great potential applications in future energy storage devices, because of its high power density, long life span and fast discharge capability.¹⁸⁻²⁰ Recently graphene-based carbonaceous materials used as electrode for supercapacitor have been investigated extensively as alternatives to the conventional graphites.²¹ Although, graphene-based electrode for supercapacitor can store and release energy rapidly and reversibly, attributed to the physical and reversible ion adsorption at the electrode/electrolyte interfaces, the low energy density of graphene limits its utility seriously. In order to address this problem, many pseudocapacitive transition-metal oxides such as MnO_2 , RuO_2 , NiO have been widely studied, because they can display more excellent electrochemical performance as the result of rapid and multiple redox reactions.²²⁻²⁶

In recent years, the fabrication of nickel sulfide used as supercapacitor electrode has been investigated extensively. Among all kinds of nickel sulfide, Ni_3S_2 has become one of the ideal active materials attributed to its excellent special capacity.²⁷⁻²⁹ Currently, Xing et al. demonstrated the electrodeposition of Ni_3S_2 on

ZnO array,³⁰ Chou et al. synthesized a flaky Ni₃S₂ nanostructure by a facile potentiodynamic deposition approach and employed the material as an electrode for supercapacitor exhibiting a specific capacitance of 717 Fg⁻¹ at 2Ag⁻¹ as well as a remarkable rate capability and excellent cycling performance.³¹ Most recently, Zhou et al. represented novel hydrothermal process to prepare Ni₃S₂ nanostructures³² and successfully deposited them on a three-dimensional (3D) graphene network, which exhibited excellent capacitive performance.³³ However, the 3D graphene template was synthesized by chemical vapor deposition process requiring the experimental temperature as high as 1000 °C. Although the preparation of graphene oxide (GO) precursor needs complicated experimental procedure, solution-processed GO has been widely used to form graphene-based composite and 3D graphene network via simple hydrothermal route for its mild synthetic conditions, as well as simple manipulation.^{34,35}

In this paper, we demonstrate a simple and facile one-step hydrothermal route to fabricate nickel sulfide/graphene nanosheets (Ni₃S₂/GNS) nanocomposites, in which graphene provides anchors for nickel sulfide nanoparticles, presents the excellent advantages structure built by pseudocapacitively nanoparticles and conducting graphene nanosheets for electrochemical performance. The prepared electrode material exhibits very high specific capacitances of 1420 Fg⁻¹ and 782 Fg⁻¹ at the current rates of 2 Ag⁻¹ and 10 Ag⁻¹, with superior cycling stability. The significant improvement of electrochemical performance is mainly attributed to the assists of graphene that provides excellent electrical conductivity and mechanical stability.

2. Experimental Section

2.1 Materials preparation

Graphene oxide was prepared from graphite powder by a simplified Hummer's method.³⁶ The Ni₃S₂/GNS electrode was obtained via the simple hydrothermal technique as follows: Typically, nickel foam was ultrasonically washed with acetone, 2 M HCl solution, deionized water, and absolute ethanol, respectively for 15 minutes, to ensure a clean nickel foam surface. The freshly washed nickel foam was then totally immersed into a 50 ml Teflon autoclave with a homogeneous solution containing 20 ml water, 10 mg GO, and 30 mg thioacetamide, (TAA, C₂H₅NS) then the mixture was heated at 180 °C for 6 h. During the autoclave was naturally cooled down to room temperature, the obtained materials were taken out, rinsed by deionized water and ethanol for several times, and dried at -55 °C for 12 h at vacuum. As a contrast, pure Ni₃S₂ and pure GNS deposited on nickel foam were also prepared under the same procedure.

2.2 Structural characterizations

Powder X-ray diffraction (XRD) data were recorded on a Rigaku D/MAX-2500 diffractometer. The surface morphologies and microstructures of resulting products were characterized by Scanning Electron Microscopy (SEM, JEOL, JSM-6360). Raman measurements were carried out by employing Renishaw in-Via micro Raman spectrometer, excited at room temperature with laser light at 532 nm.

2.3 Electrochemical tests

The electrochemical properties of the as-obtained electrode material were

investigated in a three-electrode configuration where the electrode covered with $\text{Ni}_3\text{S}_2/\text{GNS}$ nanocomposites was used as working electrode, platinum foil and Ag/AgCl served as counter and reference electrodes, respectively. All the electrochemical measurements including cyclic voltammogram, galvanostatic charge/discharge test were carried out in 1 M KOH aqueous solution with a CHI660D (ChenHua, China) electrochemistry workstation. Electrochemical impedance spectroscopy (EIS) measurement was also carried out in the frequency range of 100 kHz-0.01 Hz with perturbation amplitude of 5 mV.

3. Results and discussion

Figure 1(a) shows the XRD pattern of sample prepared in this study. Several distinct diffraction peaks at 21.7° , 31.1° , 37.7° , 50.1° and 55.3° are observed, which belong to (101), (110), (003), (211), (300) of the nickel sulfide (Ni_3S_2), respectively (JCPDS no. 44-1418). Furthermore, the other peaks can be indexed to the single nickel foam (JCPDS no.04-0850). Therefore, it is reasonable to think that the Ni_3S_2 nanoparticles have been fabricated via the hydrothermal approach. In order to further examine the crystal structures of the as-prepared samples, the Raman spectra of $\text{Ni}_3\text{S}_2/\text{GNS}$ nanocomposite, sole graphene, and pure Ni_3S_2 have been carried out, as shown in Figure 1(b). Obviously, the Raman spectra of pure Ni_3S_2 shows various peaks at $\sim 200\text{ cm}^{-1}$, $\sim 222\text{ cm}^{-1}$, $\sim 305\text{ cm}^{-1}$, $\sim 324\text{ cm}^{-1}$, 350 cm^{-1} , which can be attributed to vibration of Ni_3S_2 .³⁷ Additionally, two significant Raman peaks can be observed at 1355 cm^{-1} (D band) and 1573 cm^{-1} (G band) for GNS, corresponded to the breathing mode of A_{1g} symmetry involving phonons near the K zone boundary and

assigned to the E_{2g} mode of sp^2 -bonded carbon atoms, respectively,³⁸ extensively indicating the presence of graphene. Compared to the pure Ni_3S_2 and GNS, the above characteristic bands are all observed for the as-prepared composite sample, confirming that the Ni_3S_2 /GNS hybrid nanostructures had been successfully fabricated.

The morphologies of plain nickel foam (Supporting Information, Figure S1), pristine graphene electrode (Figure S2), and pure Ni_3S_2 (Figure S3) are characterized by Scanning Electron Microscope (SEM) test, respectively. Figure 2 shows the SEM observations of Ni_3S_2 /GNS hybrid structure. At a low magnification (Inset Figure 2(b)), the porous nickel foam network is found to be well densely and homogeneously covered by Ni_3S_2 /GNS composites. Furthermore, acting as support and spacer to prevent the agglomeration of Ni_3S_2 , the graphene nanosheets (indicated by red arrows) could be strongly and uniformly anchored by Ni_3S_2 nanoparticles, forming the special conjugated network nanostructure. The resulting electrode with individual characteristic structure may provide not only channels for electrolyte diffusion and ionic conduction toward nickel sulfide nanoparticles, but also an improvement of the active sites of redox reaction, due to the intrinsically high electrical conductivity and large network nanostructure of graphene nanosheets. All the excellent properties are proposed to benefit the reversible capacity and rate performance, leading to the extensive utilization of the obtained material applied as an electrode for supercapacitor. The EDS spectrum of Ni_3S_2 /GNS nanocomposites in Figure S4 clearly illustrates the presence of carbon (C), nickel (Ni), and sulfide (S) elements, which are

good agreement with the XRD and Raman results. According to the above results, we present the following synthesis mechanism. Via a mildly hydrothermal process, graphene oxide could be reduced to graphene nanosheets and deposit on the surface of Ni foam, forming the individual 3D graphene network simultaneously, used as template for the anchor of active material. Meanwhile, after the hydrothermal treatment, applied as Ni source, the nickel foam exposed to solution will absorb the active species (S ions) released from thioacetamide (TAA) to form small Ni₃S₂ nanoparticles anchored on the graphene nanosheets. Compared with previous report,³³ this one-step hydrothermal formation of Ni₃S₂/GNS hybrid is more facile with simple manipulation and mild synthetic conditions, and due to the active material is in-situ grown on nickel foam current collector, the electrode preparation does not require the additional polymer binder and coating procedure.³⁹

According to the cyclic voltammetry (CV) curves of Ni₃S₂/GNS at various scan rates as shown in Figure 3(a), a couple of obvious redox peaks can be observed, corresponding to the reaction between Ni²⁺/Ni³⁺ and anions OH⁻,^{30,39} indicating the typically reversible pseudocapacitive reactions, which largely contributes to the overall specific capacitance. That is very different from the fairly rectangular CV curves of graphene-based electrode, for instance, the CV plots of pure GNS prepared under the same procedure shown in Figure S5(a), which is caused by the charge separation taking place between electrode and electrolyte interface, known as double-layer capacitance behavior.^{1,40,41} Moreover, along with the rise of scan rate, the height of redox reaction peaks increases linearly and a progressive shift of the peaks

to higher voltage is presented, demonstrating that the fast redox reactions occur at the interface between active material and electrolyte. Besides, the linear relationship of the square root of the scan rate dependence of the oxidation peak current at different scan rates is shown in Figure 3(b), implying that it is a diffusion-controlled process and reversible. Even the scan rate increases to 20 mVs^{-1} , the shape of CV curves retains well, illustrating that the as-obtained electrode material has desirable pseudocapacitive property, which is generally required by power devices. To be compared, the CV test of pure Ni_3S_2 was also carried out, and the obvious similar redox peaks were observed in Figure S5(b).

Figure 4(a) and Figure S6(b) present the typical discharge curves of $\text{Ni}_3\text{S}_2/\text{GNS}$ nanocomposites and pure Ni_3S_2 at galvanostatic current densities of 2, 3, 4, 6, 8, 10 Ag^{-1} in the potential range of 0-0.5 V, respectively. Apparently, well-defined plateaus region during the discharge processes can be observed, which is consistent with the results of above CV measurements, suggesting that the as-prepared sample has excellent pseudocapacitive behaviors. Different from above results, the charge-discharge curves of pure GNS electrode (Figure S6(a)) were fairly symmetric and linear, again demonstrating the double-layer capacitance behavior. As a contrast, Figure 4(b) shows the specific capacitance of $\text{Ni}_3\text{S}_2/\text{GNS}$ and pure Ni_3S_2 electrode materials in accordance with the charge-discharge curves at different current densities. The $\text{Ni}_3\text{S}_2/\text{GNS}$ electrode delivers specific capacitances of 1420 Fg^{-1} and 782 Fg^{-1} at the current densities of 2 Ag^{-1} and 10 Ag^{-1} in 1 M KOH aqueous solution, which is much higher than those of the sole Ni_3S_2 electrode at the same current densities,

implying the superior high-rate capability of hybrid nanostructure.

Cycling capability or cycling life is a significant parameter to examine the electrochemical performance of electrode for supercapacitor application. In order to examine the cyclability of the as-prepared electrode, consecutive galvanostatic charge-discharge experiment for 2000 cycles at high current density of 6 Ag^{-1} is conducted in 1 M KOH with a potential window of 0-0.50 V. As shown in Figure 5(a), although a slight decrease in the initial stage is observed due to the active materials could not be fully used, the overall specific capacitance maintains fairly static, which is still able to achieve 994.4 Fg^{-1} after 2000 cycles. The last twenty charge-discharge curves of $\text{Ni}_3\text{S}_2/\text{GNS}$ are displayed (Inset Figure 5(a)), which indicates that the as-obtained $\text{Ni}_3\text{S}_2/\text{GNS}$ electrode holds excellent long-term electrochemical cyclability even under fast charge-discharge conditions. All together, the above experimental data demonstrates that the as-prepared $\text{Ni}_3\text{S}_2/\text{GNS}$ composites are promising candidate for designing high-performance supercapacitors.

The further electrochemical performance is investigated by electrochemical impedance spectroscopy (EIS). Nyquist plot was obtained in 1 M KOH at frequency from 100 kHz to 0.01 Hz, with an amplitude of 5 mV, which are illustrated in Figure 5(b), with a fitted equivalent circuit (inset) and an enlarged view (inset). Similar to previous report,⁴² the Nyquist plot is composed of three parts: the intersection point with the real x axis indicative of the internal resistances of the electrode (R_s), the semicircle at a relative high frequency section implying the charge-transfer resistance (R_{ct}) at the electrode-electrolyte interface and a linear region at low frequency part

corresponding to typical capacitor behavior. Notably, the Ni₃S₂/GNS nanocomposites present a smaller internal resistance (R_s) (1.14 Ω) than that (1.72 Ω) of pure Ni₃S₂, a semicircles with smaller diameter, representative of lower charge transfer resistance, and a steeper straight line with a phase angle of 74.48° larger than that (56.88°) of pure Ni₃S₂, showing the pronounced capacitive behavior with smaller diffusion resistance, due to the addition of GNS. Therefore, the low charge-transfer resistance and superior capacitive performance of Ni₃S₂/GNS nanocomposites enable fast redox reaction and easier electron transport, implying its broad application prospects in supercapacitors.

The improvement of electrochemical performance and high cycling stability of the Ni₃S₂/GNS nanocomposites is proposed to be attributed to the following aspects. Firstly, graphene nanosheets in the composite can provide not only enough anchors for nickel sulfide nanostructures, as well as effective pass-ways allowing the fast and facile ion charge transfer, due to the large network nanostructure and superior conductivity of graphene. Furthermore, the Ni₃S₂/GNS hybrid structure has been directly deposited on nickel foam substrate, which used as binder-free electrode can avoid the increase of contact resistance between active material and collector.

4. Conclusion

In summary, we have fabricated the Ni₃S₂/GNS nanocomposites and employed them as electrode materials for supercapacitor. With excellent cycle stability, the obtained electrode delivers high specific capacitances of 1420 Fg⁻¹ and 782 Fg⁻¹ at constant current rates of 2 Ag⁻¹ and 10 Ag⁻¹, respectively. Owing to accompany of

graphene nanosheets, the Ni₃S₂/GNS electrode exhibits excellent improvement of electrochemical properties, due to its large network nanostructure and high conductivity. Therefore, we conclude that the as-prepared nanocomposites present exciting potentials for electrochemical energy storage applications.

Acknowledgments

This work was supported by the Grants from National Natural Science Foundation of China (Nos. 51002129 and 51172191), Open Fund based on innovation platform of Hunan colleges and universities (No. 13K045), Provincial Natural Science Foundation of Hunan (No. 14JJ3079) , China Postdoctoral Science Foundation funded project (No. 20100480068) and Program for Changjiang Scholars and Innovative Research Team in University (IRT13093).

References

1. L. L. Zhang, X. Zhao, M. D. Stoller, Y. Zhu, H. Ji, S. Murali, Y. Wu, S. Perales, B. Clevenger and R. S. Ruoff, *Nano letters*, 2012, 12, 1806-1812.
2. Y. Qian, I. M. Ismail and A. Stein, *Carbon*, 2014, 68, 221-231.
3. X. Huang, X. Qi, F. Boey and H. Zhang, *Chemical Society reviews*, 2012, 41, 666.
4. X. Huang, Z. Zeng, Z. Fan, J. Liu and H. Zhang, *Advanced Materials*, 2012, 24, 5979-6004.
5. Q. He, S. Wu, Z. Yin and H. Zhang, *Chemical Science*, 2012, 3, 1764.
6. Z. Yin, J. Zhu, Q. He, X. Cao, C. Tan, H. Chen, Q. Yan and H. Zhang, *Advanced Energy Materials*, 2014, 4, n/a-n/a.
7. X. Huang, Z. Yin, S. Wu, X. Qi, Q. He, Q. Zhang, Q. Yan, F. Boey and H. Zhang, *Small*, 2011, 7, 1876-1902.
8. X. Cao, Y. Shi, W. Shi, G. Lu, X. Huang, Q. Yan, Q. Zhang and H. Zhang, *Small*, 2011, 7, 3163-3168.
9. X. Cao, Z. Yin and H. Zhang, *Energy & Environmental Science*, 2014, 7, 1850-1865.
10. Y. J. Mai, J. P. Tu, C. D. Gu and X. L. Wang, *Journal of Power Sources*, 2012, 209, 1-6.
11. N. Mahmood, C. Zhang and Y. Hou, *Small*, 2013, 9, 1321-1328.
12. J. Meng, H.-C. Wu, J.-J. Chen, F. Lin, Y.-Q. Bie, I. V. Shvets, D.-P. Yu and Z.-M. Liao, *Small*, 2013, 9, 2240-2244.
13. S. Das, P. Sudhagar, S. Nagarajan, E. Ito, S. Y. Lee, Y. S. Kang and W. Choi, *Carbon*, 2012, 50, 4815-4821.
14. W. Zhao, X. Zhou, Z. Xue, B. Wu, X. Liu and X. Lu, *Journal of Materials Science*, 2012, 48, 2566-2573.
15. X. Cao, Z. Zeng, W. Shi, P. Yep, Q. Yan and H. Zhang, *Small*, 2013, 9, 1703-1707.
16. X. Dong, Y. Cao, J. Wang, M. B. Chan-Park, L. Wang, W. Huang and P. Chen, *RSC Advances*, 2012, 2, 4364-4369.
17. S. Chen, J. Zhu, H. Zhou and X. Wang, *RSC Advances*, 2011, 1, 484-489.
18. B. Yuan, C. Xu, D. Deng, Y. Xing, L. Liu, H. Pang and D. Zhang, *Electrochimica Acta*, 2013, 88, 708-712.
19. Y. Q. Zhang, L. Li, S. J. Shi, Q. Q. Xiong, X. Y. Zhao, X. L. Wang, C. D. Gu and J. P. Tu, *Journal of Power Sources*, 2014, 256, 200-205.
20. X.-h. Xia, J.-p. Tu, Y.-j. Mai, X.-l. Wang, C.-d. Gu and X.-b. Zhao, *Journal of Materials Chemistry*, 2011, 21, 9319-9325.
21. G. Wang, X. Sun, F. Lu, H. Sun, M. Yu, W. Jiang, C. Liu and J. Lian, *Small*, 2012, 8, 452-459.
22. H. Zhao, F. Liu, G. Han, Z. Liu, B. Liu, D. Fu, Y. Li and M. Li, *Journal of Solid State Electrochemistry*, 2013.
23. C.-C. Hu, K.-H. Chang, M.-C. Lin and Y.-T. Wu, *Nano letters*, 2006, 6, 2690-2695.
24. Y. Jiang, D. Chen, J. Song, Z. Jiao, Q. Ma, H. Zhang, L. Cheng, B. Zhao and Y. Chu, *Electrochimica Acta*, 2013, 91, 173-178.
25. Y. Luo, D. Kong, J. Luo, S. Chen, D. Zhang, K. Qiu, X. Qi, H. Zhang, C. M. Li and T. Yu, *RSC Advances*, 2013, 3, 14413-14422.
26. C.-Y. Cao, W. Guo, Z.-M. Cui, W.-G. Song and W. Cai, *Journal of Materials Chemistry*, 2011, 21, 3204-3209.
27. T. Zhu, H. B. Wu, Y. Wang, R. Xu and X. W. D. Lou, *Advanced Energy Materials*, 2012, 2,

- 1497-1502.
28. H. Zhang, X. Yu, D. Guo, B. Qu, M. Zhang, Q. Li and T. Wang, *ACS applied materials & interfaces*, 2013, 5, 7335-7340.
 29. X. Liu, X. Qi, Z. Zhang, L. Ren, Y. Liu, L. Meng, K. Huang and J. Zhong, *Ceramics International*, 2014.
 30. Z. Xing, Q. Chu, X. Ren, C. Ge, A. H. Qusti, A. M. Asiri, A. O. Al-Youbi and X. Sun, *Journal of Power Sources*, 2014, 245, 463-467.
 31. S. W. Chou and J. Y. Lin, *Journal of the Electrochemical Society*, 2013, 160, D178-D182.
 32. W. Zhou, X.-J. Wu, X. Cao, X. Huang, C. Tan, J. Tian, H. Liu, J. Wang and H. Zhang, *Energy & Environmental Science*, 2013, 6, 2921-2924.
 33. W. Zhou, X. Cao, Z. Zeng, W. Shi, Y. Zhu, Q. Yan, H. Liu, J. Wang and H. Zhang, *Energy & Environmental Science*, 2013, 6, 2216-2221.
 34. L. Ren, X. Qi, Y. Liu, Z. Huang, X. Wei, J. Li, L. Yang and J. Zhong, *Journal of Materials Chemistry*, 2012, 22, 11765-11771.
 35. Y. Xu, K. Sheng, C. Li and G. Shi, *ACS nano*, 2010, 4, 4324-4330.
 36. W. S. Hummers Jr and R. E. Offeman, *Journal of the American Chemical Society*, 1958, 80, 1339-1339.
 37. Z. Cheng, H. Abernathy and M. Liu, *The Journal of Physical Chemistry C*, 2007, 111, 17997-18000.
 38. A. Ferrari and J. Robertson, *Physical review B*, 2000, 61, 14095.
 39. Z. Xing, Q. Chu, X. Ren, J. Tian, A. M. Asiri, K. A. Alamry, A. O. Al-Youbi and X. Sun, *Electrochemistry Communications*, 2013, 32, 9-13.
 40. X.-Y. Peng, X.-X. Liu, D. Diamond and K. T. Lau, *Carbon*, 2011, 49, 3488-3496.
 41. Z. Huang, H. Zhang, Y. Chen, W. Wang, Y. Chen and Y. Zhong, *Electrochimica Acta*, 2013, 108, 421-428.
 42. Y. Li, L. Cao, L. Qiao, M. Zhou, Y. Yang, P. Xiao and Y. Zhang, *Journal of Materials Chemistry A*, 2014, 2, 6540.

Figure Captions:

Figure 1. (a) X-ray diffraction pattern of Ni₃S₂/GNS. (b) Raman spectra of pure Ni₃S₂, GNS and Ni₃S₂/GNS nanocomposites.

Figure 2. Scanning electron microscope (SEM) images of Ni₃S₂/GNS nanocomposites; (Inset is the overview with low-magnification).

Figure 3. (a) Cyclic voltammetric curves of Ni₃S₂/GNS composite at various scan rates from 2 to 20 mVs⁻¹. (b) The relationship of the square root of the scan rate dependence of the oxidation peak current at different scan rates.

Figure 4. (a) Discharge curves of Ni₃S₂/GNS nanocomposites at different current densities (2, 3, 4, 6, 8, 10 Ag⁻¹). (b) Specific capacitance for the Ni₃S₂/GNS electrode and sole Ni₃S₂ at various current densities (2, 3, 4, 6, 8, 10, 12 Ag⁻¹).

Figure 5. (a) Cycling measurement at current density of 6 Ag⁻¹ (Inset is the galvanostatic charge-discharge curves of the last twenty cycles). (b) Nyquist plots for the Ni₃S₂/GNS electrode and sole Ni₃S₂ (The inset are the corresponding equivalent circuit and the partial enlarged Nyquist plots).

Figure 1

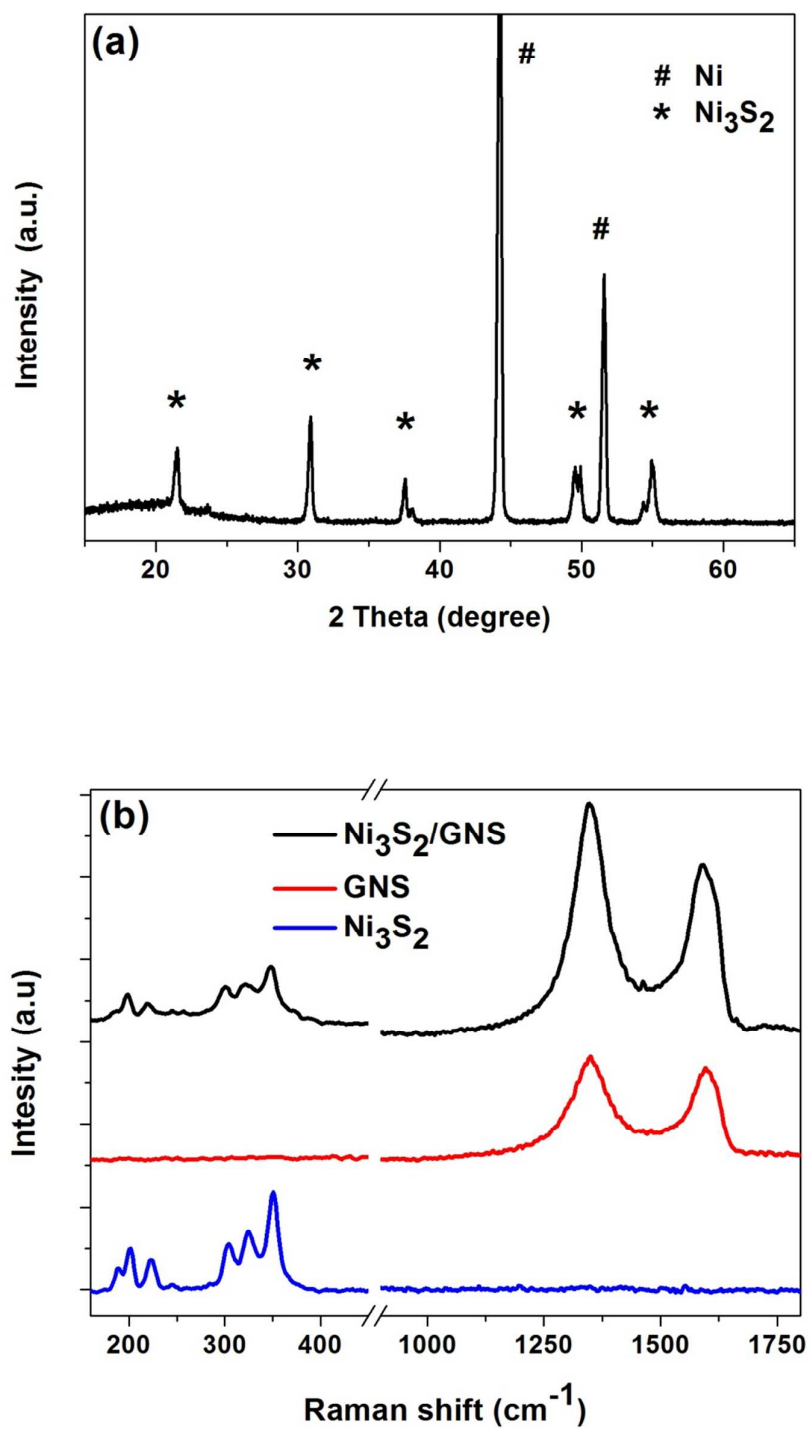


Figure 2

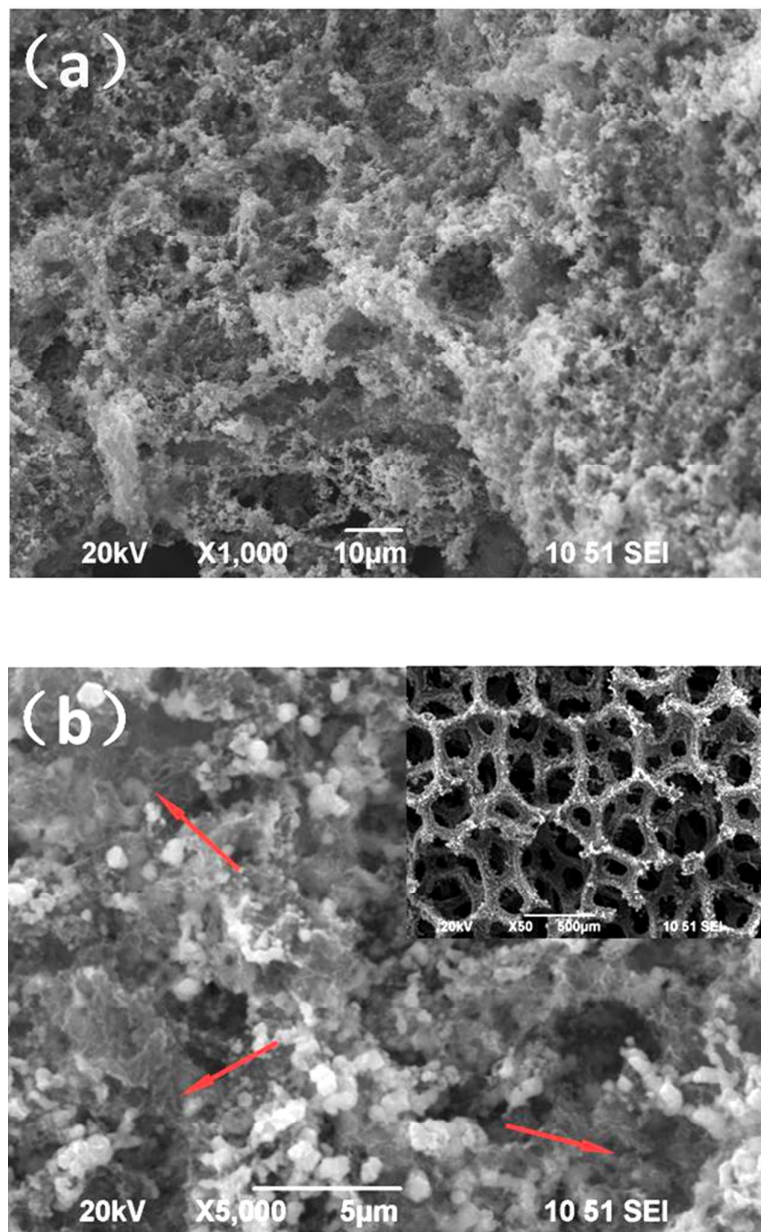


Figure 3

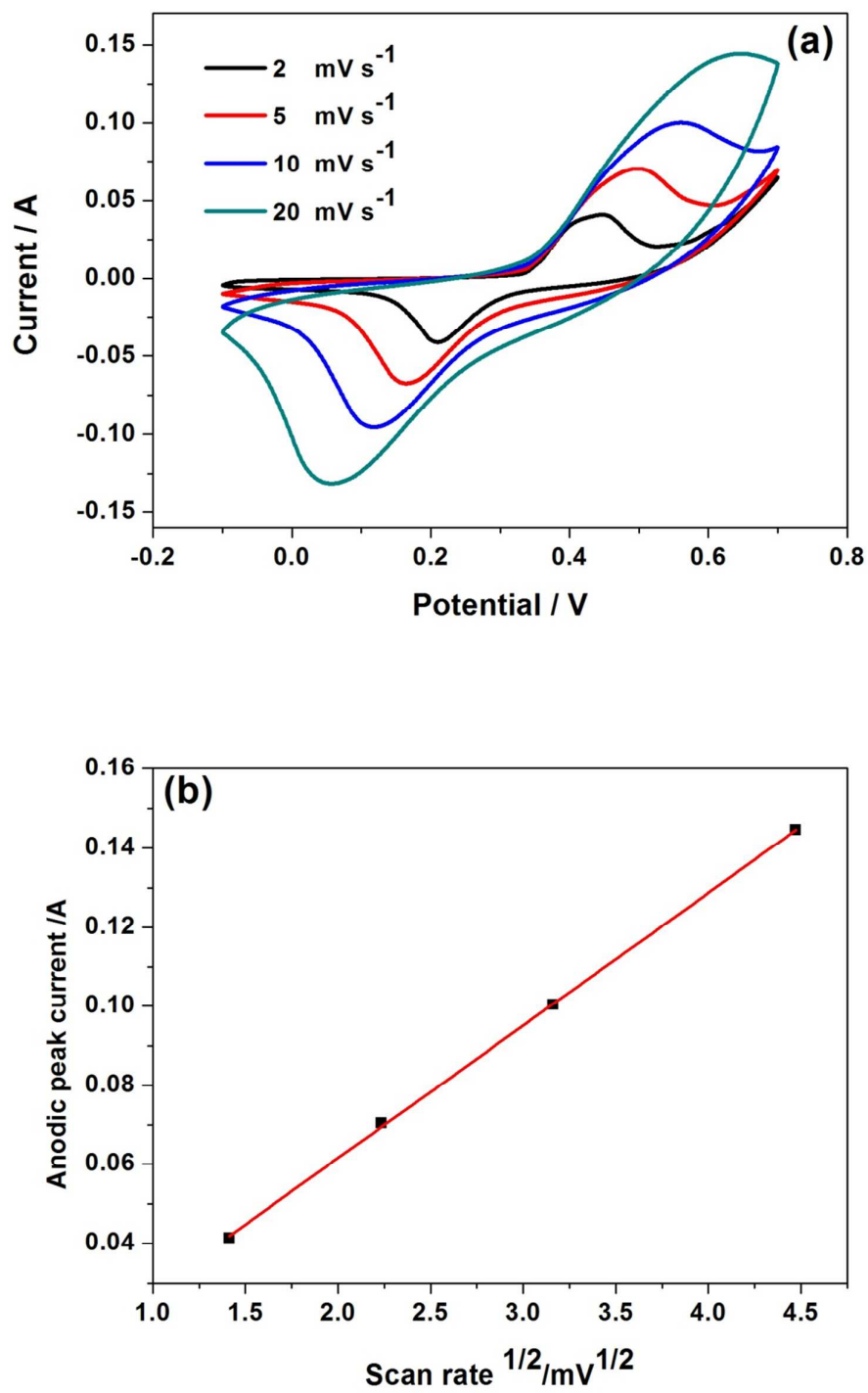


Figure 4

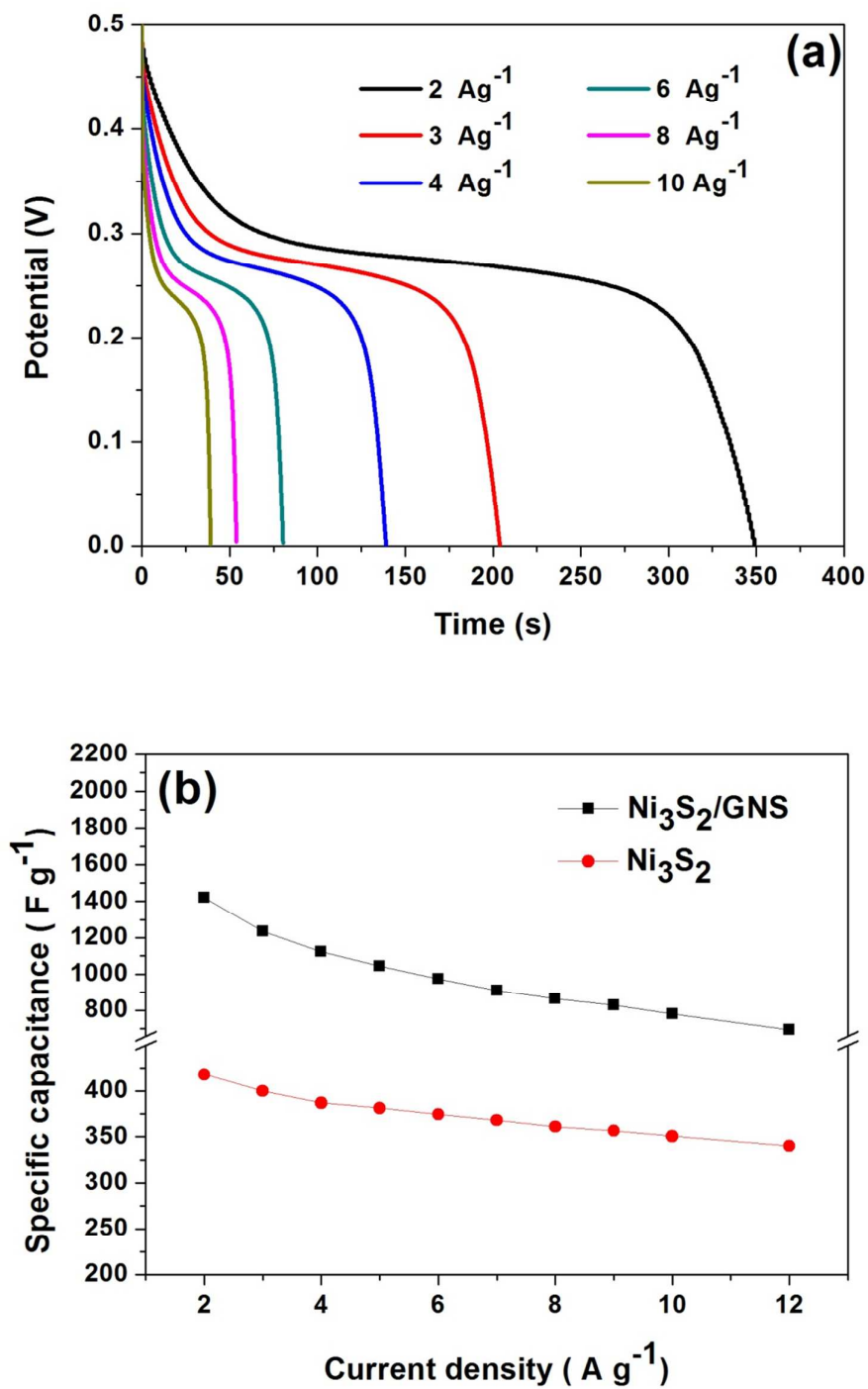


Figure 5

